Shear-Induced Structures in Semidilute Polystyrene Solution: Effect of Solvent Quality

Maya K. Endoh, Shin Saito,† and Takeji Hashimoto*

Department of Polymer Chemistry, Graduate School of Engineering, Kyoto University, Kyoto 606-8501, Japan

Received March 5, 2002

ABSTRACT: The effect of solvent quality on shear-induced structures in semidilute polystyrene solutions are investigated by using light-scattering and rheological methods. We found that the shear-induced structures are universally formed in various solvents employed in this experiment. We especially focus on a critical shear rate $\dot{\gamma}_{cx}$, at which the light scattering intensity starts to increase in our experimental geometry, and on a critical shear stress, $\sigma_{xy,cx}$, at $\dot{\gamma} = \dot{\gamma}_{cx}$. We found that $\dot{\gamma}_{cx}$ is not well correlated with χ but rather that $\sigma_{xy,cx}$ is better correlated with χ, where χ is the Flory−Huggins interaction parameter between polystyrene and solvents. $\sigma_{xy,cx}$ increases with decreasing χ. This indicates that the structure formation is strongly affected by solvent quality, mainly through the thermodynamic state of the solution. We also analyzed the solvent quality dependence of $\dot{\gamma}_{cx}$ in the context of Onuki's linear theory, and found that $\dot{\gamma}_{cx}$ can be scaled by K_{os}/η_0, where K_{os} is the osmotic modulus and η_0 the zero-shear viscosity.

1. Introduction

Shear-induced enhancement of concentration fluctuations and/or phase separation in semidilute polymer solution is now one of many intriguing phenomena not only in the field of polymer science but also in the field of nonequilibrium statistical mechanics with regard to phase transition. So far, a number of experimental and theoretical efforts have been devoted to gain an insight into the physics underlying this phenomenon.

A key concept to understand this phenomenon lies in "dynamical coupling between stress and diffusion".[1] This arises when the respective components of a binary mixture are dynamically very different, a typical example of which is a semidilute polymer solution in which polymers and solvents have slow and fast dynamics, respectively. In a semidilute polymer solution where polymers are entangled, the concentration fluctuations developed by thermal activation disturb the conformation of polymer molecules, and as a result generate local stress, because the time scale and spatial scale of the concentration fluctuations are comparable to those of the entangled polymer molecules. This local stress in turn affects the dynamics of the concentration fluctuations, triggering some interesting phenomena in semidilute polymer solutions such as the nonexponential time correlation function of the concentration fluctuations in a single phase as observed by dynamic light scattering,[2] and the viscoelastic phase separation in the thermodynamically unstable region,[3−5] as well as the shear-induced concentration fluctuations and/or phase separation of our interest in this work.[6−8]

In the case of a system subjected to shear flow, a key physical factor is the relaxation process of the spatially inhomogeneous stress induced by an externally applied shear flow. When the shear rate $\dot{\gamma}$ is smaller than the terminal relaxation rate τ_m^{-1} ($\dot{\gamma} < \tau_m^{-1}$), the local stress is relaxed via disentanglement processes of entangled polymers, and hence no enhancement of the concentration fluctuations is expected under this situation. When $\dot{\gamma} > \tau_m^{-1}$, on the other hand, the local stress, caused by the local variation of the concentration fluctuations and the concentration-dependent viscosity, is released by squeezing solvents from the regions having more entanglement points and hence larger stress. This process accompanies a further enhancement of concentration fluctuations. As $\dot{\gamma}$ is increased further, the shear-induced phase separation is eventually brought about.

In experimental studies, semidilute solutions of polystyrene in dioctyl phthalate (PS/DOP) have been exclusively employed,[6−8] because this system has the following advantages in conducting experiments: DOP is a nonvolatile solvent and PS/DOP has a phase boundary at around the room temperature. However, of course, this phenomenon should not be limited to PS/DOP. Theories[9−11] indicate that this phenomenon emerges irrespective of systems if some thermodynamic and viscoelastic conditions are satisfied as discussed later. In this study, to check universality of this phenomenon and explore the effect of the solvent quality on the structure formation, we experimentally investigated the shear-induced structure formation in semidilute polystyrene solutions with various solvents by conducting light-scattering and rheological experiments.

There are two characteristic shear rates regarding the shear-induced structure formation observed in the $q_x - q_z$ plane as a function of $\dot{\gamma}$.[12] One is $\dot{\gamma}_{cx}$, at which the light-scattering intensity along the flow direction (q_x) starts to increase in the $q_x - q_z$ plane. Here q is the amplitude of the scattering wave vector defined as $q = |\boldsymbol{q}| = (4\pi/\lambda)\sin(\theta/2)$, where λ is the wavelength of the incident beam and θ is the scattering angle in medium. The x, y, and z axes indicate, respectively, the flow direction, the velocity gradient direction, and the neutral direction, and q_x, q_y, and q_z are the respective components of $\boldsymbol{q}$. $\dot{\gamma}_{cx}$ is a shear rate from which the nonlinear enhancement of the concentration fluctuations starts to occur,[12] a basis of which is that the structure factor at $\dot{\gamma} > \dot{\gamma}_{cx}$ cannot be described by a linearized time-

* To whom correspondence should be addressed.
† Present address: Tsukuba Research Laboratory, Sumitomo Chemical Co., Ltd., Ibaraki, Tsukuba, 300-3294, Japan.

10.1021/ma0203389 CCC: $22.00
Published on Web 08/24/2002

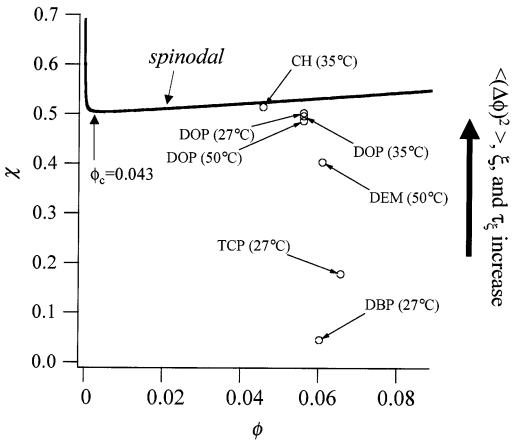

Figure 1. Phase diagram of the polystyrene solution used in this experiment in the parameter space of χ (Flory−Huggins interaction parameter between polymer and solvent), defined in eq 6 and listed in Table 2 of text, as a vertical axis and ϕ (volume fraction of polymer in the solution) as a horizontal axis. The solid line indicates the spinodal curve calculated by the Flory−Huggins theory. The calculated critical volume fraction ϕ_c is equal to 0.0043. The circles indicate the points at which the experiments were conducted. At nearly same values of ϕ (=0.46−0.61), $M = 5.48 \times 10^6$ and T (=27−50 °C) employed in this experiment, as χ increases, $\langle(\Delta\phi)^2\rangle$, ξ and τ_ξ are expected to increase, while η_0/η_s may not change much as discussed in the text.

dependent Ginzburg−Landau type dynamical equation based on a theory proposed by Helfand and Fredrickson,[9] Milner[10] and Onuki.[11] Another is $\dot{\gamma}_{cz}$, at which the light-scattering intensity along q_z starts to increase. $\dot{\gamma}_{cz}$ is believed to be a shear rate from which the shear-induced demixing starts to occur.[13,14] The characteristic shear rate concerned in this study is the former one, i.e., $\dot{\gamma}_{cx}$. In our previous study,[12] we have already elucidated the temperature and concentration dependence of $\dot{\gamma}_{cx}$ for a given solvent. The present paper would complement ref 12 with a study of the solvent quality dependence of $\dot{\gamma}_{cx}$ and the shear stress at $\dot{\gamma}_{cx}$ (defined hereafter critical shear stress $\sigma_{xy,cx}$), which is analyzed in conjunction with the Flory−Huggins interaction parameter χ. The results are also compared with a linearized theory proposed by Onuki.[11]

Before getting into the main part of this work, it would be worthy to think about how and why the solvent quality affects $\dot{\gamma}_{cx}$. As spelled out in ref 12, $\dot{\gamma}_{cx}$ strongly depends on both the thermodynamic property, which determines the nature of the concentration fluctuations in the quiescent state, and the viscoelastic property, which determines whether the stress is relaxed by disentanglement or squeezing of solvents. Thus let us briefly think about how the solvent quality affects the thermodynamic and viscoelastic properties of a solution in order to gain insight on how it affects the shear-induced structure formation. Below we first discuss the effect of the solvent quality on the thermodynamic property and then on the viscoelastic property.

The nature of the concentration fluctuations in the quiescent state is characterized by the mean-squared amplitude $\langle(\Delta\phi)^2\rangle$, the correlation length ξ, and the lifetime of the concentration fluctuations having a wavelength ξ, τ_ξ, which are determined by the position of the solution in a phase diagram shown in Figure 1, where the spinodal line of the solution to be dealt with in this study is drawn, with χ as a vertical axis and ϕ as a horizontal axis (χ and ϕ will be defined later), based

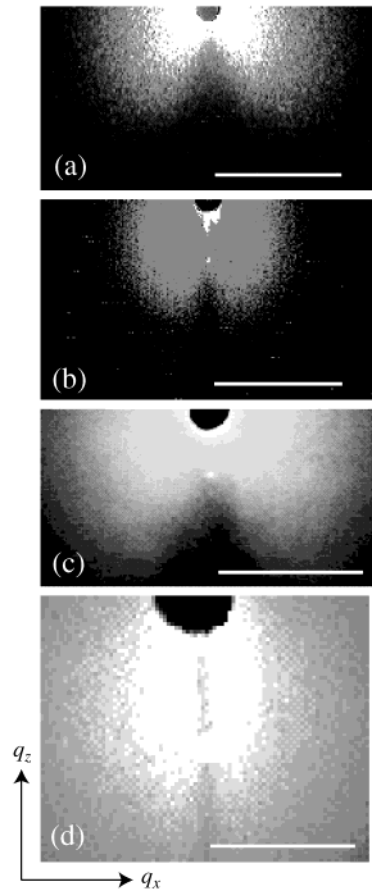

Figure 2. Scattering patterns from the semidilute solutions of polystyrene in various solvents subjected to shear flow with flow axis along horizontal direction. Bars in parts a−c represent $q = 1.0\ \mu m^{-1}$, while that for part d represents $q = 0.5\ \mu m^{-1}$. Key: (a) PS/CH at 35 °C and at $\dot{\gamma} = 1\ s^{-1}$; (b) PS/DBP at 27 °C and at $\dot{\gamma} = 316\ s^{-1}$; (c) PS/DEM at 50 °C and at $\dot{\gamma} = 100\ s^{-1}$; (d) PS/TCP at 27 °C and at $\dot{\gamma} = 316\ s^{-1}$. In each figure is shown only half of the pattern, because each pattern is symmetric with respect to the $q_x - q_y$ plane.

on the Flory−Huggins theory.

$$f = \frac{k_B T}{v_0}\left[\frac{\phi}{N}\ln\phi + (1-\phi)\ln(1-\phi) + \chi\phi(1-\phi)\right] \quad (1)$$

$$\simeq \frac{k_B T}{v_0}\left[\frac{\phi}{N}\ln\phi + \left(\frac{1}{2} - \chi\right)\phi^2 + \frac{1}{6}\phi^3\right] \quad (2)$$

Here f is the free energy density of mixing of polymers and solvents, k_B is the Boltzmann constant, v_0 the volume of a monomeric unit, ϕ the volume fraction of polymer, N the degree of polymerization of polymer, and χ the Flory−Huggins interaction parameter between polymer and solvent. The spinodal line at which $\langle(\Delta\phi)^2\rangle$, ξ, and τ_ξ diverge is obtained from the condition of $(\partial^2 f/\partial\phi^2) \equiv r_0 = 0$, where

$$r_0 = \frac{k_B T}{v_0}\left[\frac{1}{N\phi} + (1-2\chi) + \phi\right] \quad (3)$$

In the above equation, only χ depends on the solvent quality. The value of χ increases and that of r_0 decreases, as the solvent quality becomes poorer (corresponding to a shift toward the spinodal line in Figure 1 in the single phase solution) at a given polymer concentration ϕ, resulting in increases in $\langle(\Delta\phi)^2\rangle$, ξ and τ_ξ, since $\langle(\Delta\phi)^2\rangle$

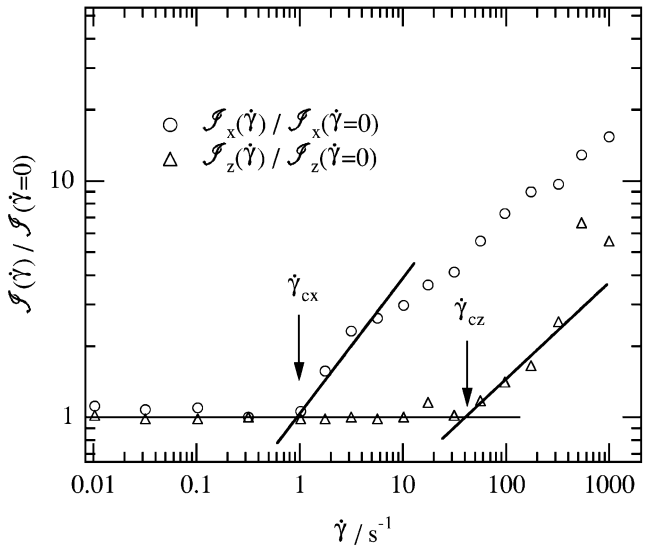

Figure 3. Normalized integrated intensities along the q_x and q_z, $\mathcal{I}_x(\dot\gamma)/\mathcal{I}_x(\dot\gamma = 0)$, and $\mathcal{I}_z(\dot\gamma)/\mathcal{I}_z(\dot\gamma = 0)$ plots, respectively, as a function of $\dot\gamma$ in double logarithmic scale. Critical shear rates $\dot\gamma_{cx}$ ($\dot\gamma_{cz}$) are determined as the value at which the two straight lines fitted to the data points of $\mathcal{I}_x(\dot\gamma)/\mathcal{I}_x(\dot\gamma = 0)$ ($\mathcal{I}_z(\dot\gamma)/\mathcal{I}_z(\dot\gamma = 0)$) intersect as shown in the figure.

$\sim r_0^{-1}$, $\xi = \sqrt{C/r_0}$ with C being constant independent of the solvent quality as defined later, and $\tau_\xi = \xi^2/D \sim \xi^3$ with D being the diffusion constant, according to the mean-field theory. We shall discuss later how the values of χ in Figure 1 are evaluated.

On the other hand, as for the viscoelastic property, the slow mechanical relaxation process is important in the shear-induced structure formation. The maximum relaxation time τ_m and the zero-shear viscosity η_0 characterize this process. Although the scaling laws of η_0 and τ_m for semidilute solutions with respect to the concentration ϕ or c (g/mL) and the molecular weight M for both good and Θ solvents are available from the extensive literature, the data on how η_0 and τ_m change with the solvent quality at a given c, M, and T are quite limited. It was reported,[15,16] however, that at higher concentrations the polystyrene solutions with Θ solvents give higher relative viscosity η_0/η_s (with η_s being the solvent viscosity) than those with good solvents, while at lower concentrations the formers give lower η_0/η_s than the latters, and the crossover concentration exists in the range $c/c^* = 2.2-4.7$ where c^* is the overlap concentration as will be defined in section 2.1 below. It follows that η_0/η_s of the solutions with Θ solvents is almost the same or slightly higher than those with good solvents at the concentration of our interest ($c/c^* = 5.1-7.4$). In the following discussion, η_0/η_s may be assumed to be almost independent of the solvent quality. More rigorously, the viscoelastic properties will be later shown in Figure 4.

2. Experimental Method

2.1. Samples. Samples employed in this study were semidilute polystyrene (PS) solutions with a given molecular weight and concentration but with various solvents. The weight average molecular weight of PS was 5.48×10^6, and the heterogeneity index for the molecular weight distribution was 1.15. The concentration of PS prepared was 6.0 wt % for all the solutions. The solvents used were dioctyl phthalate (DOP, Θ solvent for PS at 22 °C), cyclohexane (CH, Θ solvent for PS at 35 °C), diethyl malonate (DEM, Θ solvent for PS at 35 °C), dibutyl phthalate (DBP, good solvent for PS), and tricresyl phosphate (TCP, good solvent for PS).[17] The c^* value was calculated using $c^* = 3M_w/(4\pi R_g^3 N_A)$ with an assumption of R_g given by $R_g = b(N_w/6)^{0.5}$, where R_g, N_A, b, and N_w are, respectively, the radius of gyration of a single polymer molecule, Avogadro's number, the statistical segmental length (6.7 Å), and the weight average degree of polymerization. Then c/c^* values of each solution at 25 °C were 6.7 for PS/DOP, 5.1 for PS/CH, 6.9 for PS/DEM, 6.8 for DBP, and 7.4 for TCP. Thus the c/c^* covered in this work is approximately in the range 5−7.

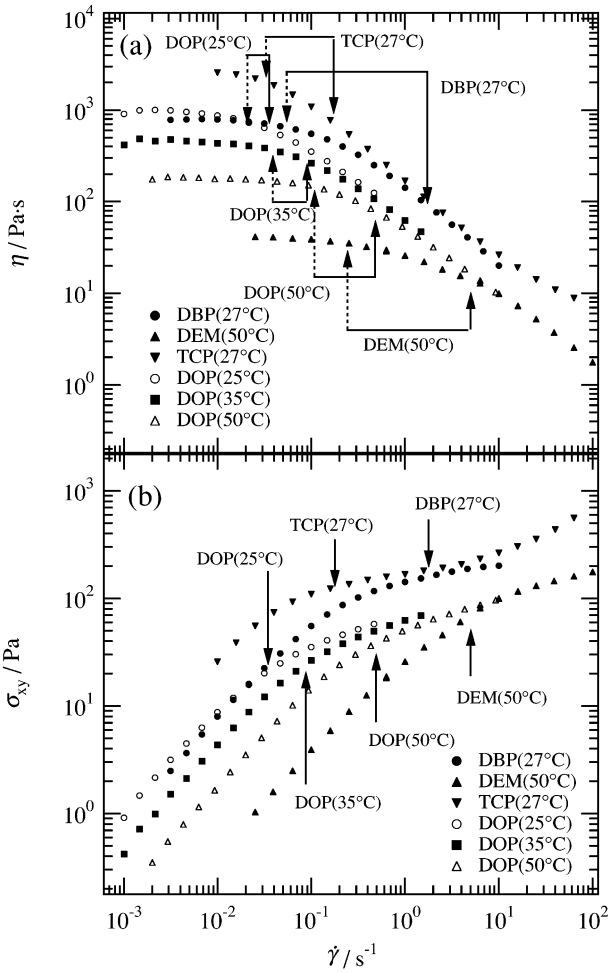

Figure 4. Steady-state shear viscosity η (a) and shear stress σ_{xy} (b) as a function of shear rate for semidilute solutions of polystyrene (with the given molecular weight and at the fixed concentration as indicated in the text) in various solvents. Solid and broken arrows in part a denote $\dot\gamma_{cx}$ and τ_m^{-1} of each solution, respectively.

2.2. Light Scattering. Two apparatuses were used to measure the light scattering intensity distribution under shear flow. One is to obtain scattering profiles as a function of q_x and q_z by using photodiode array. The details of this apparatus have been described elsewhere.[18] Another is to obtain the two-dimensional scattering patterns in the $q_x - q_z$ plane by using a CCD camera, as detailed elsewhere.[19] Both use a He−Ne laser having a wavelength of 632.8 nm as an incident beam source. The shear cell used was the same for both apparatus, a transparent cone-and-plate type shear cell made of quartz with 80 mm diameter and 1° cone angle.

2.3. Rheology. Measurements of steady-state viscosity η as a function of shear rate $\dot\gamma$ were carried out with RMS-800 and ARES−FS (Rheometric Scientific Co. Ltd.) by using cone−plate fixtures.

3. Results

3.1. Scattering Patterns. Figure 2 shows two-dimensional scattering patterns from semidilute solu-

Table 1. Values of $\dot{\gamma}_{cx}$, τ_m, τ_m^{-1}, η_0, $\sigma_{xy,cx}$, $\sigma_{xy}(\dot{\gamma} = \tau_m^{-1})$ of the Semidilute Solutions of Polystyrene in Various Solvents

solvent	$\dot{\gamma}_{cx}$ (s^{-1})	τ_m (s^{-1})	τ_m^{-1} (s^{-1})	η_0 (Pa·s)	$\sigma_{xy,cx}$ (Pa)	$\sigma_{xy}(\dot{\gamma} = \tau_m^{-1})$ (Pa)
DOP (27 °C)	3.56×10^{-2}	4.80×10^{1}	2.08×10^{-2}	8.57×10^{2}	2.04×10^{1}	1.45×10^{1}
DOP (35 °C)	8.98×10^{-2}	2.48×10^{1}	4.03×10^{-2}	4.53×10^{2}	2.42×10^{1}	1.49×10^{1}
DOP (50 °C)	5.01×10^{-1}	8.58	1.17×10^{-1}	1.78×10^{2}	3.71×10^{1}	1.69×10^{1}
CH (35 °C)	5.62×10^{-1}	3.49×10^{-2} [a]	2.87[a]	3.73×10^{1} [a]		
DEM (50 °C)	5.01	3.96	2.53×10^{-1}	4.03×10^{1}	7.07×10^{1}	9.03
TCP (27 °C)	1.78×10^{-1}	3.02×10^{1}	3.32×10^{-2}	2.65×10^{3}	1.26×10^{2}	6.72×10^{1}
DBP (27 °C)	1.78	1.78×10^{1}	5.61×10^{-2}	7.88×10^{2}	2.32×10^{2}	3.70×10^{1}

[a] Obtained from ref 21.

tions with various solvents under steady state shear. In the quiescent state, the scattering pattern is isotropic and the intensity is very weak. Under shear flow, the scattering intensity is highly enhanced and the scattering excess to that from quiescent solution gives the patterns as shown in Figure 2. The scattering patten becomes anisotropic with two lobes of high intensity along the flow direction (parallel to q_x), which is called "butterfly", provided that the shear rate is higher than a certain critical shear rate $\dot{\gamma}_{cx}$ which depends on the solvent used. The butterfly pattern is a characteristic of the shear-induced enhancement of concentration fluctuations and/or phase separation. It should be stressed in this figure that the butterfly patterns are observed for all the solutions, irrespective of the solvent species, although the temperature and shear rate required are different.[17] This indicates that the shear-induced structure formation is a universal phenomenon for semidilute polystyrene solutions.

3.2. Determination of Critical Shear Rate. To determine the critical shear rate $\dot{\gamma}_{cx}$, we introduce an integrated intensity along q_x as follows:

$$\mathcal{I}_x(\dot{\gamma}) = \int_{q_{x,\min}}^{q_{x,\max}} I(q_x;\dot{\gamma})\, dq_x \qquad (4)$$

Here $I(q_x;\dot{\gamma})$ is the scattering intensity distribution along q_x at a given $\dot{\gamma}$, $q_{x,\min}$ ($=3.17 \times 10^{-4}$ nm^{-1}) and $q_{x,\max}$ ($=3.68 \times 10^{-3}$ nm^{-1}) are the lower and upper limits of the experimental q window along q_x. The integrated intensity along q_z, $\mathcal{I}_z$, was also introduced in order to determine the critical shear rate $\dot{\gamma}_{cz}$ by replacing $q_{x,\min}$ and $q_{x,\max}$ with $q_{z,\min}$ ($=3.26 \times 10^{-4}$ nm^{-1}) and $q_{z,\max}$ ($=3.58 \times 10^{-3}$ nm^{-1}), respectively, and q_x with q_z in eq 4. Figure 3 shows a typical example of the double logarithmic plot of $\mathcal{I}_x$ and $\mathcal{I}_z$ as a function of $\dot{\gamma}$ obtained for PS/DBP solution at 27 °C, where $\mathcal{I}_x$ and $\mathcal{I}_z$ are normalized with respect to those in the quiescent state, i.e., $\mathcal{I}_x(\dot{\gamma} = 0)$ and $\mathcal{I}_z(\dot{\gamma} = 0)$, respectively. $\mathcal{I}_x$ and $\mathcal{I}_z$ dramatically increase when $\dot{\gamma}$ is increased above the critical shear rate, indicated by the vertical arrows marked by $\dot{\gamma}_{cx}$ and $\dot{\gamma}_{cz}$, respectively. The critical shear rate along q_x (q_z), defined as $\dot{\gamma}_{cx}$ ($\dot{\gamma}_{cz}$), is assessed as $\dot{\gamma}$ above which $\mathcal{I}_x/\mathcal{I}_x(\dot{\gamma} = 0)$ ($\mathcal{I}_z/\mathcal{I}_z(\dot{\gamma} = 0)$) starts to deviate from unity. More precisely, $\dot{\gamma}_{cx}$ ($\dot{\gamma}_{cz}$) is determined as the value at which the two straight lines intersect each other as shown in Figure 3. All other PS solutions with different solvents and at different temperatures had similar $\dot{\gamma}$ dependence of $\mathcal{I}_x$ and $\mathcal{I}_z$, enabling the determination of $\dot{\gamma}_{cx}$ and $\dot{\gamma}_{cz}$ with almost same accuracy. In this work, however, we focuses only on $\dot{\gamma}_{cx}$ and $\sigma_{xy,cx}$. $\dot{\gamma}_{cx}$ values thus determined are summarized in Table 1.

3.3. Determination of Zero-Shear Viscosity and Maximum Relaxation Time. Figure 4a shows the steady shear viscosity η as a function of $\dot{\gamma}$ for the systems for which the shear–light-scattering experiments were performed. Data for PS/DOP at 25 °C are presented instead of those at 27 °C, at which the light-scattering experiment was carried out. The zero-shear viscosity η_0 and the maximum relaxation time τ_m were obtained by fitting the following Carreau function to η:[20]

$$\eta = \eta_0[1 + (\dot{\gamma}\tau_m)^2]^{-a} \qquad (5)$$

Here a is the shear-thinning exponent. η_0 and τ_m obtained as fitting parameters are also summarized in Table 1 along with the critical shear stress at $\dot{\gamma}_{cx}$, $\sigma_{xy,cx}$, and the shear stress at τ_m^{-1}, $\sigma_{xy}(\dot{\gamma} = \tau_m^{-1})$. The broken arrows in part a indicate the value $\dot{\gamma}$ corresponding to the value τ_m^{-1} evaluated by the fitting of η vs $\dot{\gamma}$ with eq 5, while the solid arrows indicate $\dot{\gamma}_{cx}$ which was defined in section 3.2. The viscoelastic data for PS/DOP at 27 °C in Table 1 were obtained as interpolated values of the viscoelastic data measured from 20 to 50 °C by 5 °C steps.[12] Data for PS/CH were evaluated by using scaling relations on η_0 and τ_m at 35 °C with respect to concentration and molecular weight investigated by Adam and Delsanti.[21] Figure 4b shows the shear stress σ_{xy} as a function of $\dot{\gamma}$. Arrows in Figure 4b denote $\dot{\gamma}_{cx}$ of each solution. Figure 5 represents a master curve of η/η_0 vs $\dot{\gamma}a_T$ at 27 °C for PS/DOP which was evaluated by the time–temperature superposition principle[22] (a) and the corresponding shift factor a_T as a function of reciprocal temperature (b) in which data at temperatures other than 25, 35, and 50 °C is presented.

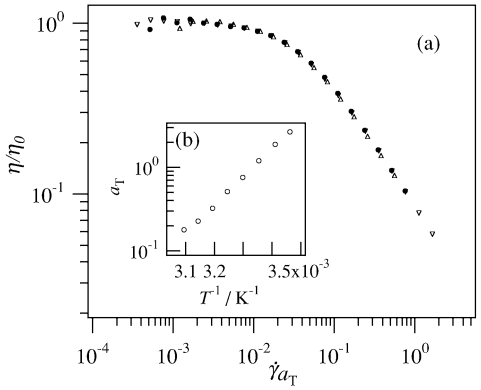

Figure 5. Master curve of η/η_0 vs $\dot{\gamma}a_T$ for PS/DOP at 27 °C obtained by time–temperature superposition of η vs $\dot{\gamma}$ in Figure 4a (a) and temperature dependence of the shift factor a_T (b).

3.4. Relationship between $\dot{\gamma}_{cx}$ and τ_m^{-1}. To clarify the relationship between $\dot{\gamma}_{cx}$ and τ_m^{-1}, $\dot{\gamma}_{cx}$ in Table 1 is plotted as a function of τ_m^{-1} in Figure 6. The characteristic rates are clearly correlated in such a way that $\dot{\gamma}_{cx}$ increases with increasing τ_m^{-1}. $\dot{\gamma}_{cx}$ may obey a power law of $\dot{\gamma}_{cx} \sim (\tau_m^{-1})^{\alpha}$ with an exponent of $\alpha \simeq 2$. It is also worth noting that $\dot{\gamma}_{cx}$ lies in $\dot{\gamma}_{cx} > \tau_m^{-1}$, indicating that the shear-induced structure formation starts to occur after the nonlinearity of the viscoelastic behavior becomes remarkable. The relation between τ_m^{-1} and $\dot{\gamma}_{cx}$

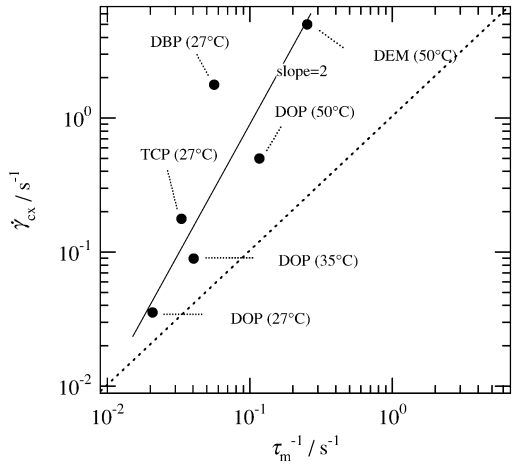

Figure 6. $\dot{\gamma}_{cx}$ as a function of reciprocal maximum relaxation rate τ_m^{-1}. The dotted line indicates $\dot{\gamma}_{cx} = \tau_m^{-1}$.

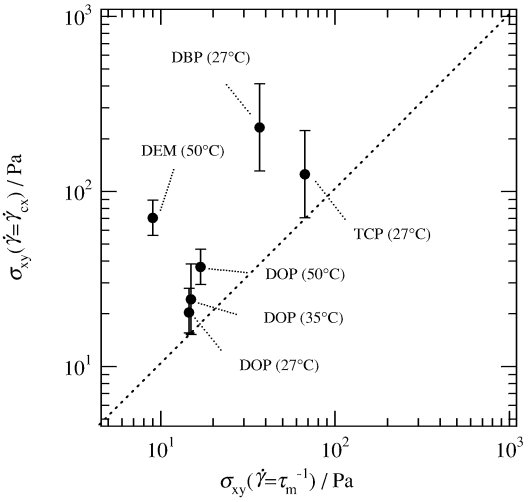

Figure 7. Critical shear stress at $\dot{\gamma}_{cx}$, $\sigma_{xy,cx}$, as a function of shear stress at τ_m^{-1}, $\sigma_{xy}(\dot{\gamma} = \tau_m^{-1})$. The dotted line indicates $\sigma_{xy,cx} = \sigma_{xy}(\dot{\gamma} = \tau_m^{-1})$.

was represented by means of the broken and solid arrows in Figure 4.

3.5. Relationship between $\sigma_{xy,cx}$ and $\sigma_{xy}(\dot{\gamma} = \tau_m^{-1})$. To clarify the relationship between $\sigma_{xy,cx}$ and $\sigma_{xy}(\dot{\gamma} = \tau_m^{-1})$, $\sigma_{xy,cx}$ in Table 1 is plotted as a function of $\sigma_{xy}(\dot{\gamma} = \tau_m^{-1})$ in Figure 7. Though $\sigma_{xy,cx}$ increases with increasing $\sigma_{xy}(\dot{\gamma} = \tau_m^{-1})$, a systematic correlation between them cannot be discerned, indicating that the critical stress for the structure formation is not necessarily related fully to the rheological critical stress. All the data points satisfy $\sigma_{xy,cx} > \sigma_{xy}(\dot{\gamma} = \tau_m^{-1})$, also indicating that the shear-induced structure formation starts to occur after the onset of nonlinearity in the viscoelastic behavior.

4. Discussion

It would be intuitively obvious that the shear-induced structure should depend on solvent quality, simply because solvent quality affects amplitude, correlation length and lifetime of thermal concentration fluctuations. We already discussed in detail some anticipated effects of solvent quality on shear-induced structure in section 1. To qualitatively check our intuition concerning the effects, we shall discuss correlation between segmental interaction χ and $\dot{\gamma}_{cx}$ in section 4.2 and correlation between χ and $\sigma_{xy,cx}$ in section 4.3, both free from any models or theories. A more elaborated analysis of $\dot{\gamma}$ and $\sigma_{xy,cx}$, based upon a theoretical model, shall be discussed in section 5.

Table 2. Values of χ Obtained from Literatures, K_{os} and K_{os}/η_0 for Semidulute Solutions of Polystyrene in Various Solvents

solvent	χ	K_{os} (Pa)	K_{os}/η_0 (s^{-1})
DOP (27 °C)	0.503	3.73×10^3	4.35
DOP (35 °C)	0.497	4.76×10^3	1.05×10^1
DOP (50 °C)	0.487	6.61×10^3	3.71×10^1
DEM (50 °C)	0.404	2.01×10^4	4.99×10^2
TCP (27 °C)	0.179 (χ_H)	5.26×10^4	1.98×10^1
DBP (27 °C)	0.0457 (χ_H)	7.28×10^4	9.23×10^1

4.1. Evaluation of χ. To find a systematic correlation between the shear-induced structure formation and the solvent quality, we focus on the χ parameter between polystyrene and solvent. It should be noted, however, that χ reflects only the thermodynamic aspect of a solution, though χ, together with the viscoelastic properties, should play an important role on the shear-induced structure formation on a quantitative basis as will be discussed in section 5.

χ is given as follows:

$$\chi = \chi_H + \chi_S \tag{6}$$

Here χ_H and χ_S are the enthalpic and entropic components of the thermodynamic interactions.

The values of χ were obtained from the literature as follows:

(1) For PS/DOP, Nicolai and Brown[23] have studied χ as a function of concentration and temperature by static light scattering. We rearranged their data to plot χ as a function of the reciprocal temperature T^{-1}, and found χ linearly depends on T^{-1} as $\chi = 0.277 + 67.8/T$ for 6.0 wt % in the temperature range from 10 to 50 °C, which corresponds to the range of our experiment.

(2) For PS/DEM, Song and Torkelson[24] have obtained a cloud point curve. The PS used has M_w of 2.9×10^5 and $M_w/M_n \leq 1.06$. By regarding it as a binodal curve and neglecting the concentration dependence of χ, we obtained χ as a function of temperature as $\chi = -0.898 + 420/T$.

(3) For PS/TCP and PS/DBP, the experimental χ values are not available. We therefore use χ_H evaluated below instead of χ, but this is quite problematic, since χ_S cannot be neglected for almost all the pairs of polymer and solvent.

χ_H is given as follows:[25]

$$\chi_H = \frac{V_s}{RT}(\delta_s - \delta_p)^2 \tag{7}$$

Here V_s is the molar volume of the solvent, R is the gas constant, and δ_p and δ_s are the solubility parameters of polymer and solvent, respectively. Calculations of χ_H were done using δ_i (i = p (polymer) or i = s (solvent)) calculated by the group contribution method, as detailed in Appendix. δ_s, $(\delta_s - \delta_p)^2$, and χ_H thus calculated are tabulated in Table 2.

4.2. $\dot{\gamma}_{cx}$ and χ. In Figure 8, $\dot{\gamma}_{cx}$ is plotted as a function of χ. At a first glance $\dot{\gamma}_{cx}$ is not well correlated with χ as typically shown for the set of data for the DOP solutions at 27, 35, and 50 °C as well as that for DEM (50 °C). For them the $\dot{\gamma}_{cx}$ values vary despite the fact that the χ values are approximately identical. For these solvents with nearly constant χ values, $\dot{\gamma}_{cx}$ seems to increase with decreasing η_0 as found in Table 1. It means that the

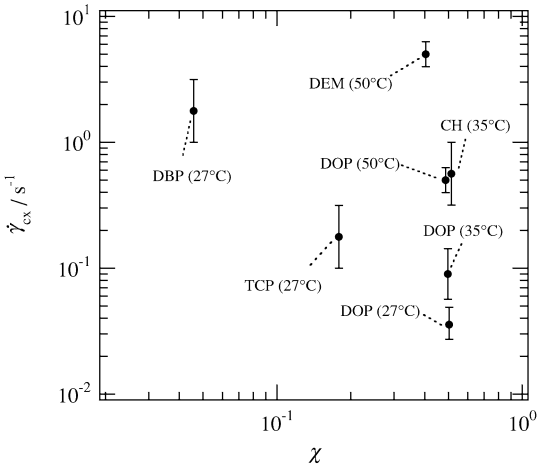

Figure 8. $\dot{\gamma}_{cx}$ as a function of χ.

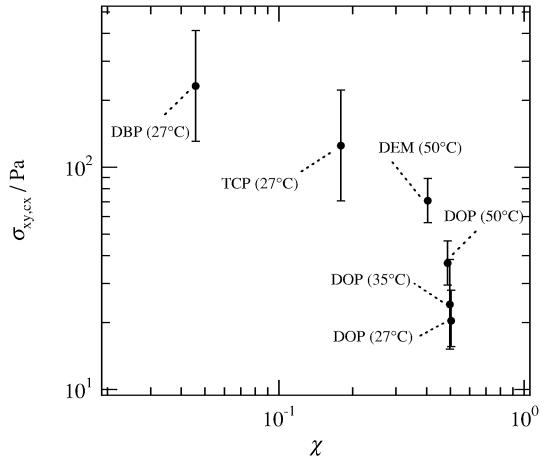

Figure 9. $\sigma_{xy,cx} = \sigma_{xy}(\dot{\gamma} = \dot{\gamma}_{cx})$ as a function of χ.

shear-induced structure formation occurs at a higher shear rate for the solvent giving rise to a lower value of η_0, if the solvents under consideration have nearly identical χ values. Thus the stress levels seem to be an important parameter for the shear-induced structure formations for these systems. However the three data at 27 °C (data for DBP(27 °C), TCP(27 °C), and DOP(27 °C)) indicate that $\dot{\gamma}_{cx}$ tends to systematically decrease with increasing χ. This trend is reasonable, since the poorer the solvent quality (the higher the value of χ), the larger and longer the spatial and time scale of the concentration fluctuations, respectively, and hence the more the stress-diffusion coupling or the resulting solvent squeezing process, required for the shear-induced structure formation, becomes effective at a lower shear rate.

Let us further compare the data of $\dot{\gamma}_{cx}$ of DBP, TCP and DOP solutions at 27 °C. Note that these are the data obtained at the same concentration, molecular weight and temperature. At $\dot{\gamma} = 3.56 \times 10^{-2}$ s^{-1} (which corresponds to $\dot{\gamma}_{cx}$ for the DOP solution at 27 °C), the stress level of DBP and TCP solutions are higher than that of DOP (as seen in Figure 4(b), for example). Thus if the average stress level $\langle\sigma_{xy}\rangle$ is crucial for the shear-induced fluctuations, the shear-induced structure should be already formed at this shear rate in the DBP and TCP solutions. This is because the shear stresses of the DBP and TCP solutions at $\dot{\gamma} = \dot{\gamma}_{cx}$(DOP, 27°C) $= 3.56 \times 10^{-2}$ s^{-1} are higher than that of DOP solution. However, the experimental results reveal that the DBP and TCP solutions do not still have the shear-induced structures and that $\dot{\gamma}_{cx}$ for the TCP and DBP solutions are higher than that of the DOP solution. This indicates that at a given c, M, and T, what is important for the onset of the shear-induced structure formation is not the average stress level $\langle\sigma_{xy}\rangle$, but rather the nature of the concentration fluctuations and the resulting local stress variations $\nabla\sigma_{xy}$. In the DBP and TCP solutions at $\dot{\gamma} = \dot{\gamma}_{cx}$(DOP, 27°C), the stress level is higher than that for DOP (27 °C), but the local stress variations may not be large enough to develop the shear-induced fluctuations. Thus a higher shear rate and a higher shear stress level are required for these solutions. In this way the critical shear rate and critical shear stress themselves depend on solvent quality or χ. As $\langle(\Delta\phi)^2\rangle$, ξ, and τ_ξ increase (i.e., as χ increases along the arrow in Figure 1), the solution becomes sensitive to the local stress buildup and its spatial variation, which further trigger the shear-induced fluctuations via the stress relaxation induced by squeezing of solvents. This effect lowers $\dot{\gamma}_{cx}$, explaining the trend in Figure 8 for the three solvents.

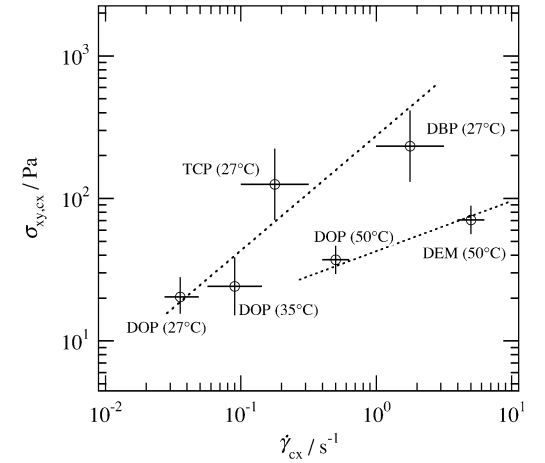

Figure 10. $\sigma_{xy,cx}$ as a function of $\dot{\gamma}_{cx}$ for DOP (27 °C), TCP (27 °C), DBP (27 °C), DOP (35 °C), DOP (50 °C), and DEM (50 °C).

4.3. Critical Shear Stress, $\sigma_{xy,cx}$, and χ. In Figure 9, $\sigma_{xy,cx}$ is plotted as a function of χ. $\sigma_{xy,cx}$ tends to decrease with increasing χ, indicating that the higher critical stress level is needed as the solvent quality becomes better. The change in $\sigma_{xy,cx}$ with χ is more systematic than that in $\dot{\gamma}_{cx}$ with χ in Figure 8, because the data points obtained at approximately equal χ values are collapsed nearly at the same value of $\sigma_{xy,cx}$. This result is consistent with the solvent-squeezing model introduced in section 1. As χ increases, $\langle(\Delta\phi)^2\rangle$, ξ, and τ_ξ increase, giving rise to the higher local variation of the stress or the higher imbalance in the stress. The local stress buildup or the stress imbalance tends to be relaxed by the solvent-squeezing, which enhances the concentration fluctuations. This enhancement occurs at a lower $\dot{\gamma}$ and hence at a lower stress, as χ increases. It should be noted that $\sigma_{xy,cx}$ is detected as a spatially averaged value of this locally fluctuating stress.

4.4. $\sigma_{xy,cx}$ and $\dot{\gamma}_{cx}$. In Figure 10, $\sigma_{xy,cx}$ is plotted as a function of $\dot{\gamma}_{cx}$ for DOP (27 °C), TCP (27 °C), DBP (27 °C), DOP (35 °C), DOP (50 °C), and DEM (50 °C). It is qualitatively concluded that $\sigma_{xy,cx}$ increases with increasing $\dot{\gamma}_{cx}$ from the data obtained for different solvents at a given temperature, e.g., a set of data for DOP (27 °C), TCP (27 °C), and DBP (27 °C) or a set of data for DOP (50 °C) and DEM (50 °C). This trend may be best

interpreted as a consequence of the fact that the better the solvent, the larger the values of $\dot{\gamma}_{cx}$ and the larger the values of $\sigma_{xy,cx}$.

5. Comparison with Theory

5.1. Theory. At this stage, we try to analyze $\dot{\gamma}_{cx}$ in a more quantitative way than in the previous section. Helfand-Fredrickson, Milner, and Onuki proposed a dynamical equation in order to account for the shear-induced enhancement of concentration fluctuations based on a two-fluid model (HFMO theory).[9−11] The HFMO theory provides $\dot{\gamma}_{cx}$ within a linear approximation. In this section, we briefly introduce Onuki's theory[11] and theoretically derive $\dot{\gamma}_{cx}$.

According to the HFMO theory, the dynamics of the concentration fluctuations is described by the following time-dependent Ginzburg−Landau type equation where the coupling between stress and diffusion is included:

$$\left(\frac{\partial}{\partial t} + \boldsymbol{v}\cdot\nabla\right)\phi = \nabla\cdot L\left[\nabla\frac{\delta F}{\delta\phi} - \frac{1}{\phi}\nabla\cdot\sigma^{(n)}\right] + \theta_\phi \qquad (8)$$

Here $\boldsymbol{v}$ is the average velocity of the polymer and the solvent, ϕ the volume fraction of polymer, L the Onsager coefficient, F the free energy functional, $\sigma^{(n)}$ the stress tensor on the entangled network, and θ_ϕ the thermal noise contribution. On the assumption that $\sigma^{(n)}$ is expressed by the deviatopic part of the mechanical stress tensor derived for the Newtonian fluids, we can establish a linear equation for the Fourier components $\phi_{\mathbf{q}}$

$$\left(\frac{\partial}{\partial t} - \dot{\gamma} q_x \frac{\partial}{q_y}\right)\phi_{\mathbf{q}} = - L_{\mathrm{eff}}(q)\left[q^2(r_0 + Cq^2) - \frac{2\eta_0'}{\phi}\dot{\gamma} q_x q_y\right]\phi_{\mathbf{q}} + \theta_{\mathbf{q}} \qquad (9)$$

where r_0 is defined in eq 3, C, the coefficient for the term accounting for the energy cost of concentration inhomogeneity (concentration gradient), is given by the random-phase approximation, $\theta_{\mathbf{q}}$ is the contribution of the thermal noise of the $\boldsymbol{q}$ Fourier mode satisfying the fluctuation−dissipation theorem, and $\eta_0' = \partial\eta_0/\partial\phi$. $L_{\mathrm{eff}}(q)$ is the q-dependent Onsager coefficient, given by $L_{\mathrm{eff}}(q) = L/(1 + q^2\xi_{\mathrm{ve}}^2)$, where ξ_{ve} is the viscoelastic length representing the strength of coupling between stress and diffusion:[1] $\xi_{\mathrm{ve}} = (4L\eta_0/3\phi^2)^{0.5} = (4D_{\mathrm{co}}\eta_0/3K_{\mathrm{os}})^{0.5}$, where D_{co} and K_{os} are, respectively, the cooperative diffusion constant and the osmotic modulus, though the detail of ξ_{ve} is not important in this work.

From eq 9, we obtain the following relaxation rate of the concentration fluctuation at a given q-mode:

$$\Gamma_{\mathrm{eff}}(\boldsymbol{q}) = L\left[q^2(r_0 + Cq^2) - \frac{2\eta_0'}{\phi}\dot{\gamma} q_x q_y\right]/[1 + \xi_{\mathrm{ve}}^2 q^2] \qquad (10)$$

Here r_0 is positive for metastable or stable solutions above the spinodal point. When $\Gamma_{\mathrm{eff}} < 0$, the sheared solution becomes thermodynamically unstable and the steady-state structure factor cannot be obtained. Hence, $\Gamma_{\mathrm{eff}} = 0$ at small q yields a stability limit. Under the condition of $q_x = q_y = q/\sqrt{2}$, for example, the critical shear rate $\dot{\gamma}_c$ for the shear-induced instability is given by

$$\dot{\gamma}_c \cong \frac{r_0\phi}{\eta_0'} = \frac{\phi^2 r_0}{5\eta_0} = \frac{K_{\mathrm{os}}}{5\eta_0} \qquad (11)$$

where $K_{\mathrm{os}}(\equiv \phi(\partial\pi/\partial\phi) = \phi^2 r_0)$ is the osmotic modulus. In this work, we asuume that this critical shear rate $\dot{\gamma}_c$ obtained in this theory is propotional to that obtained in this experiment $\dot{\gamma}_{cx}$, i.e., $\dot{\gamma}_{cx} \propto \dot{\gamma}_c$, though the critical shear rate in our experiment may reflect the shear rate above which the nonlinear enhancement of the concentration fluctuations starts to occur.[12] On this assumption, $\dot{\gamma}_{cx}$ is proportional to K_{os}/η_0, surely reflecting the expectation discussed in section 1 that the shear-induced structure formation depends on both the thermodynamic (K_{os}) and the viscoelastic (η_0) properties.

Here we have to stress that eq 11 is derived on the special assumption, regarding viscoelasticity, such that the solution is a Newtonian fluid and $N_1 = 0$ over all the shear rates covered. This assumption is problematic since $\dot{\gamma}_{cx} > \tau_{\mathrm{m}}^{-1}$ as shown in Figure 4 and N_1 cannot be negligible at $\dot{\gamma}_{cx}$. Hereafter we continue our analysis using eq 11 despite this problem, because eq 11 is reasonable and useful when comparing the experimental results with a theory.

5.2. Determination of K_{os}. To estimate $\dot{\gamma}_c$ in eq 11 experimentally, we have to evaluate the values of K_{os}. K_{os} for a semidilute solution is given by[11]

$$K_{\mathrm{os}} = \left(\frac{k_{\mathrm{B}}T}{v_0}\right)\phi^2\left[\phi + (1 - 2\chi) + \frac{1}{N_{\mathrm{n}}\phi}\right], \qquad (12)$$

where N_{n} is the number average polymerization index and χ is the segmental interaction parameter given by eq 6 and tabulated in Table 2 for the system studied in this work. The values of K_{os} and K_{os}/η_0 thus obtained are also summarized in Table 2.

It is ideal to actually measure K_{os} using light scattering and compare the measured values with those estimated here. However accurate determination of K_{os} for the semidilute solutions with the large molecular weight in our studies, espescially for good solvents such as TCP and DBP, simply because they yield scattering intensity much weaker than DOP as expected from Figure 1. Thus we would like to leave this measurement for future works.

5.3. $\dot{\gamma}_{cx}$ as a Function of K_{os}/η_0. Figure 11 shows a double logarithmic plot of $\dot{\gamma}_{cx}$ against K_{os}/η_0 where $\dot{\gamma}_{cx}$ increases with increasing K_{os}/η_0 according to a power law with an exponent of unity. This is in excellent agreement with eq 11, indicating that the shear-induced enhancement of concentration fluctuation depends on both the thermodynamic and viscoelastic properties. Despite the serious assumption on χ mentioned in the previous section, the data points of DBP (27 °C) and TCP (27 °C) are roughly on the dotted line with a slope of unity. This may be due to the fact that the contribution of χ_S on K_{os} is insensitive concerning this plot. However it should be noted that the absolute values of $\dot{\gamma}_{cx}$ are systematically lower than those of $\dot{\gamma}_c$ in eq 11 by a factor of about 10.

Thus we have found that Onuki's linear theory can describe not only the temperature and concentration dependence of $\dot{\gamma}_{cx}$, as studied in our previous paper,[12] but also the dependence of $\dot{\gamma}_{cx}$ on the solvent quality. The parameter that remains to be studied is the molecular weight. The molecular weight dependence of $\dot{\gamma}_{cx}$ would be also reduced by K_{os}/η_0 as far as $c > c^*$,

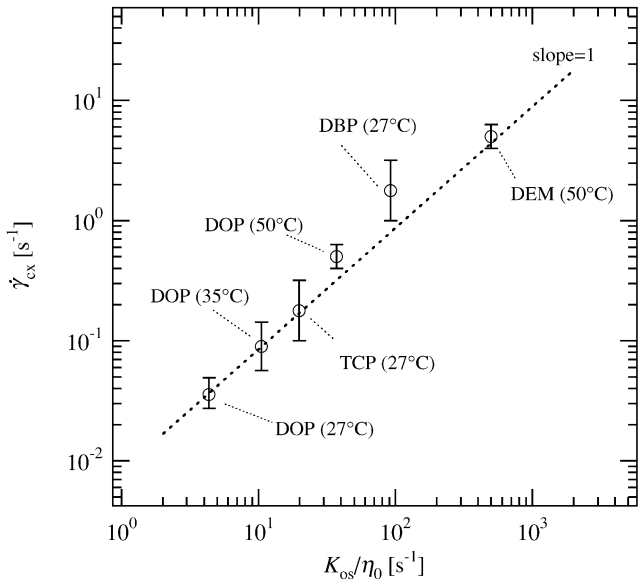

Figure 11. $\dot{\gamma}_{cx}$ as a function of K_{os}/η_0. The dotted line indicates the theoretical prediction with slope 1.

which is required to hold the thermodynamic and viscoelastic relations of a semidilute solution.

6. Summary

We have investigated the effect of solvent quality on the shear-induced structure formation in semidilute polystyrene solutions. We have found out that this phenomenon is common for polystyrene solutions with various solvents. In a qualitative analysis of $\dot{\gamma}_{cx}$ focusing on only the thermodynamic interaction parameter χ, $\dot{\gamma}_{cx}$ and the corresponding shear stress $\sigma_{xy,cx}$ increased with decreasing χ, revealing that the higher shear rate and shear stress are needed for the shear-induced structure formation as the solvent quality becomes better. We also discussed that the local stress fluctuations $\nabla\sigma_{xy}$ is dominant in terms of the structure formation over the average of the locally fluctuating stress that is detectable by the rheological experiment. The important finding of this article was that the dependence of the solvent quality on $\dot{\gamma}_{cx}$ could be scaled by K_{os}/η_0 in accordance with Onuki's linear theory: $\dot{\gamma}_{cx}$ increased in proportion to K_{os}/η_0, indicating that the shear-induced structure formation depends on both the thermodynamic and viscoelastic properties. We expect that a trend similar to that found for $\dot{\gamma}_{cx}$ will be observed also for $\dot{\gamma}_{cz}$, the critical shear rate for the onset of demixing. The discussion on $\dot{\gamma}_{cz}$, however, will be left for future work.

Appendix

The solubility parameters used are calculated by using the group contribution method.[26] The solubility parameter δ_i is defined as

$$\delta_i = \sqrt{\frac{\Delta E_i^v}{V_i}} \tag{A1}$$

where ΔE_i^v is the energy of vaporization per mole of the i-th molecule (either a solvent or polymer), and V_i is its molar volume. In the group contribution method, it is assumed that the contributions of different functional groups in a molecule to the thermodynamic property are additive. Small[27] defined the molar attraction constant F_{ij} for each functional group j in the i-th molecule as

$$\sum_j F_{ij} = (\Delta E_i^v V_i)^{1/2}. \tag{A2}$$

Substituting (A2) into (A1) yields

$$\delta_i = \left(\frac{\Delta E_i^v V_i}{V_i^2}\right)^{1/2} = \frac{\sum_j F_{ij}}{V_i} = \frac{\rho_i \sum_j F_{ij}}{M_i} \tag{A3}$$

where ρ_i and M_i are the density and molecular weight of the i-th molecule, respectively. Sets of values of F_{ij} are available in ref 26.

References and Notes

(1) Doi, M.; Onuki, A. *J. Phys. II Fr.* **1992**, *2*, 1631.
(2) Brown, W.; Nicolai, T. In *Dynamic Light Scattering*; Brown, W., Ed.; Clarendon Press: Oxford, U.K., 1993.
(3) Tanaka, H. *Phys. Rev. Lett.* **1993**, *71*, 3158.
(4) Tanaka, H. *J. Phys., Condens. Matter.* **2000**, *12*, 207.
(5) Toyoda, N.; Takenaka, M.; Saito, S.; Hashimoto, T. *Polymer* **2001**, *42*, 9193.
(6) Hashimoto, T.; Fujioka, K. *J. Phys. Soc. Jpn.* **1991**, *60*, 356.
(7) Wu, X.-L.; Pine, D. J.; Dixon, P. K. *Phys. Rev. Lett.* **1991**, *66*, 2408.
(8) Yanase, H.; Moldenaers, P.; Mewis, J.; Abetz, V.; van Egmond, J.; Fuller, G. G. *Rheol. Acta* **1991**, *30*, 89.
(9) Helfand, E.; Fredrickson, G. H. *Phys. Rev. Lett.* **1989**, *62*, 2468.
(10) Milner, S. T. *Phys. Rev. E* **1993**, *48*, 3674.
(11) Onuki, A. *J. Phys., Condens. Matter.* **1997**, *9*, 6119.
(12) Saito, S.; Hashimoto, T. *J. Chem. Phys.* **2001**, *114*, 10531.
(13) Morfin, I.; Lindner, P.; Boué F. *Macromolucules* **1999**, *32*, 7208.
(14) Saito, S.; Hashimoto T.; Morfin, I.; Lindner, P.; Boué, F. *Macromolucules* **2002**, *35*, 445.
(15) Simha, R.; Zakin, J. L. *J. Colloid Sci.* **1962**, *17*, 270.
(16) Gandhi, K. S.; Williams, M. C. *J. Polymer Sci.* **1971**, *35*, 211.
(17) In this experiment, we used the data for the system of PS/CH at 35 °C only to show qualitatively the general feature that the shear-induced structure is observed for various solvents. All the quantitative analyses were done with other nonvolatile or less-volatile solvents.
(18) Hashimoto, T.; Takebe, T.; Suehiro, S. *Polym. J.* **1986**, *18*, 123.
(19) Kume, T.; Asakawa, K.; Moses, E.; Matsuzaka, K.; Hashimoto, T. *Acta Polym.* **1995**, *46*, 79.
(20) Bird, R. B.; Armstrong, R. C.; Hassager, O. *Dynamics of Polymeric Liquids*; Wiley: New York, 1977.
(21) Adam, M.; Delsanti, M. *J. Phys.* **1984**, *45*, 1513.
(22) Ferry, J. D. *Viscoelastic Properties of Polymers*, 2nd ed.; Wiley: New York, 1970.
(23) Nicolai, T.; Brown, W. *Macromolucules* **1996**, *29*, 1698.
(24) Song, S.-W.; Torkelson, J. M. *Macromolecules* **1994**, *27*, 6389.
(25) Hildebrand, J. H.; Scott, R. L. *The Solubility of Nonelectrolytes*; Reinhold: New York, 1959.
(26) *Polymer Handbook*, 4th ed.; Brandup, J., Immergut, E. H., Grulke, E. A., Eds.; Wiley: New York, 1999.
(27) Small, P. A. *J. Appl. Chem* **1953**, *3*, 71.

MA0203389